Cleaner Chemical Engineering 12 (2025) 100209

Contents lists available at ScienceDirect

Cleaner Chemical Engineering

journal homepage: www.elsevier.com/locate/clce

Ultrasound-assisted esterification of cotton cellulose with long chain free fatty acids

Pierre Dal [a], Annelise Jean-Fulcrand [a], Jean-Marc Lévêque [b], Jean-Marie Raquez [a], Daria C. Boffito [a,c,*]

[a] Polytechnique Montreal, Dept. Chemical Engineering, CP 6079, Succ CV, Montreal, QC H3C 3A7, Canada
[b] Laboratoire rhéologie et procédés, Université Grenoble Alpes, 363 rue de la chimie, 38400 Saint-Martin-d'Hères, France
[c] Canada Research Chair in Engineering Process Intensification and Catalysis (EPIC), Polytechnique Montreal, Canada

ARTICLE INFO

Keywords:
Cellulose
Esterification
Free fatty acids
Ultrasound
Sonochemistry
COMSOL

ABSTRACT

This work covers the production of cellulose esters with varying degrees of substitution (*DS*) using ultrasound (US) power input, leveraging free fatty acids as esterification agent (*EA*) as a bio-based alternative to traditional chlorides, anhydrides and vinyl esters. The best conditions without US were achieved with oleic acid, with an *EA*/cellulose molar ratio of 6 and a temperature of 80 °C for 24 h, producing esters with a *DS* of 1.44. Applying US at 20 kHz and 4.39 W at room temperature, required <30 min to produce cellulose esters with a *DS* of 0.38. Then, the effects of the US input power, reaction volume and properties of cellulose solutions on the cavitation activity were investigated by simulations in COMSOL. The density, viscosity and speed of sound in the cellulose esters solutions were measured and defined in the simulations as 936.2 kg m^{-3}, 23.3·10^{-3} Pa.s, and 1495.8 m s^{-1} for 25 g L^{-1}. Simulations with conditions resulting in the highest *DS* with US were characterized by the smallest acoustic cavitation volume and the lowest *u*: 9.60·10^{-8} m^3 and 40.06 m s^{-1}. US-assisted esterification produced thermoplastic esters with an energy input of 18 W g^{-1} of cellulose against 93 W g^{-1} required by conventional esterification.

1. Introduction

Cellulose, the most abundant bio-based polymer, serves as the primary structural component of plant cell walls. It is composed of anhydroglucose units (AGUs) connected by glycosidic bonds. Due to its extensive hydrogen bonding network, cellulose exhibits poor solubility and is difficult to process in most organic solvents or in its molten state. Transforming waste cellulose into esters with thermoplastic properties presents a sustainable alternative to petroleum-based thermoplastics. Long-chain cellulose esters with a degree of substitution (*DS*) greater than 0.7 exhibit thermoplastic behavior and can be processed without the need for plasticizer (Edgar et al., 2001).

Traditional esterification reactions can be carried out in either homogeneous or heterogeneous phases. Homogeneous reactions typically produce esters with a controlled *DS* (Tanaka et al., 2017) and a uniform distribution of functional groups along the cellulose chains (Zhang et al., 2015). However, these esterification reactions use lithium chloride/N, N-dimethylacetamide (LiCl/DMAc) as a solvent, which is expensive, difficult to recycle (Willberg-Keyriläinen and Ropponen, 2019), non-volatile and toxic (Mikkola et al., 2007). In the case of heterogeneous esterification, it involves an excess of esterification agent (*EA*) and pyridine or sulfuric acid as a catalyst (Zhang et al., 2015). However, it results several drawbacks, including uneven functionalization, low *DS*, long reaction times (5 h to 16 h) (Willberg-Keyriläinen and Ropponen, 2019), side reactions (Zhang et al., 2015) and degradation of cellulose (Heinze et al., 2006).

Common esterification agents (*EAs*) include chlorides, anhydrides (Sejati et al., 2024b, 2024a), and vinyl esters (Willberg-Keyriläinen and Ropponen, 2019). Chlorides release hydrochloric acid (HCl), which is corrosive and degrades the cellulose and esters (Vaca-Garcia and Borredon, 1999; Willberg-Keyriläinen and Ropponen, 2019). Anhydrides produce cellulose esters with low *DS* in LiCl/DMAc. Vinyl esters require the removal of the vinyl alcohol formed (Willberg-Keyriläinen and Ropponen, 2019).

As an alternative, free fatty acids (FFA) offer several key advantages: they are derived from biomass, use mild reaction conditions and

* Corresponding author at: Polytechnique Montreal, Dept. Chemical Engineering, CP 6079, Succ CV, Montreal, QC H3C 3A7, Canada.
E-mail address: daria-camilla.boffito@polymtl.ca (D.C. Boffito).

https://doi.org/10.1016/j.clce.2025.100209
Received 7 April 2025; Received in revised form 13 September 2025; Accepted 22 September 2025
Available online 24 September 2025

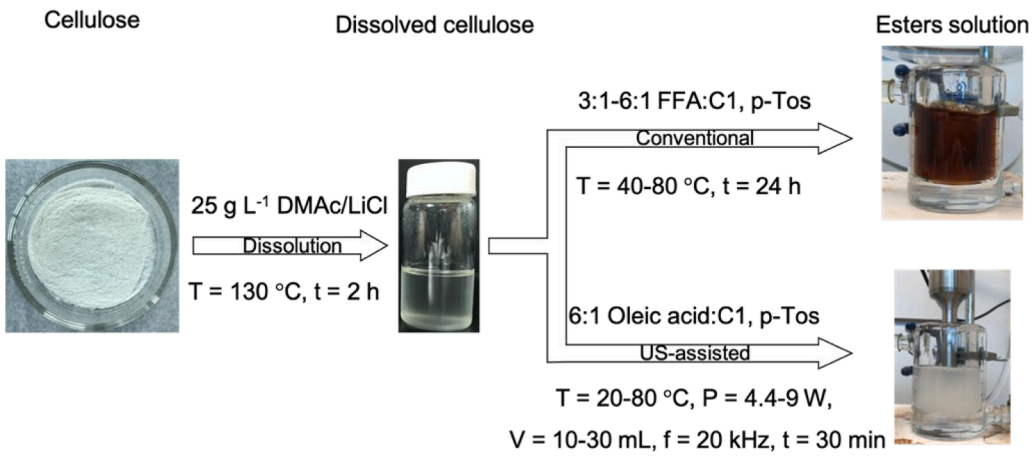

Fig. 1. Cellulose dissolution and esterification steps, for conventional or US-assisted method. Precipitation in ethanol follows the esterification.

generate limited by-products (Daulay et al., 2024; X. Huang et al., 2019; Kulomaa et al., 2015; Willberg-Keyriläinen and Ropponen, 2019). Unlike other esterification routes, FFA do not degrade cellulose chains but require an activating agent to increase their reactivity (Willberg-Keyriläinen and Ropponen, 2019). For instance, Willberg-Keyriläinen and Ropponen (2019) esterified cellulose with various *EA* in LiCl/DMAc, achieving the highest *DS* (1.3) with octanoyl chloride. However, it generated HCl, requiring neutralization by N, N-dimethyl-4-aminopyridine (DMAP) to prevent cellulose from hydrolysis (Duchatel-Crépy et al., 2020). Vinyl esters produced the lowest *DS* (below 0.1) and required the removal of the vinyl alcohol formed.

Using p-toluenesulfonyl chloride (p-Tos) as an activating agent alongside 3-(hydroxyphenylphosphinyl)-propanoic acid enabled to produce thermoplastic esters with a *DS* of 1.42 in LiCl/DMAc at 40 °C in 24 h (Zheng et al., 2015). Similarly, Almasi et al. (2015) produced cellulose nanofibers esters in pyridine and p-Tos, achieving a *DS* of 1.82, with oleic acid at 50 °C for 4 h. Uschanov et al. (2011) esterified cotton linters cellulose with oleic acid for 4 h, resulting into a *DS* of 1.25, while Costa et al. (2023) obtained α-cellulose esters with a *DS* of 2.45 with stearic acid, at 80 °C for 5 h.

Process intensification (PI) csnenhance efficiency by reducing plant size, cutting costs and energy use by 20–80 %, and decreasing chemical consumption by factors of 10 to 1000 (Fernandez Rivas et al., 2020). Mechanochemistry such as ball milling, is an example of PI for cellulose esterification. Huang et al. (2019) obtained a *DS* of 0.041 after 150 min at 500 rpm, with acetic anhydride improving oleic acid reactivity. Hou et al. (2021) esterified MCC in DMAc with DMAP, EDCHCl, and oleic acid, reaching a *DS* of 2.55 after 4 h at 500 rpm. Lease et al. (2021) produced esters with a *DS* of 0.21 from MCC, oleic acid and p-Tos in 1-butyl-3-methylimidazolium acetate using a magnetic mortar at 100 °C for 12 h, preserving cellulose crystallinity. They attributed the low *DS* to surface modification rather than bulk esterification.

Ultrasound (US) is a PI technology that has proven to intensifiy processes via macro shear rates and acoustic cavitation. The implosion of cavitation bubbles creates extreme localized conditions, with temperature of ~5 000 K, pressure up to 500 atm, fluid microjets, and reactive radicals (Suslick, 1990). These conditions improve heat and mass transfer, and accelerate chemical reactions, especially esterification (Boffito et al., 2014). In liquid-liquid systems, US emulsifies phases, increasing interfacial surface area and reaction rates (Meroni et al., 2022). In liquid-solid systems, cavitation bubbles collapse on solid surfaces, producing high-speed jets, localized temperatures and pressures, and enhancing liquid-solid mass transfer (Mikkola et al., 2004).

US has been rarely used for cellulose dissolution and esterification, because extended sonication can reduce molecular weight by cleaving polymer linkages (Grönroos et al., 2004). At 525 kHz, high-frequency US selectively depolymerizes MCC into glucose at 60 °C by generating H• and •OH radicals inside the cavitation bubbles, from the unmodified cellulose and solvent (Haouache et al., 2020). These radicals break glycosidic bonds on the cellulose surface. Bhaumik and Dhepe (2015) noted that US irradiation disrupts hydrogen bonds and reduces cellulose crystallinity, as US energy exceeds the 21 kJ mol^{-1} required for hydrogen bond dissociation (Bochek, 2003).

Treating cellulose with US decreased the dissolution time by 68 % (Lan et al., 2011) to 92 % (Mikkola et al., 2007) compared to silent conditions. However, regenerated cellulose after US showed a 28 % drop in degree of polymerization (DP) compared to cellulose dissolved without US (Lan et al., 2011). In another study, US simultaneously degraded and esterified cellulose pulp into NCC at 40 kHz during 5 h at 70 °C, increasing yield by 77 % and *DS* by 110 % compared to silent conditions (Tang et al., 2013). They attributed this behavior to selective degradation of the amorphous regions, improving reagent accessibility to the internal structure of cellulose, as US energy (10–100 kJ mol^{-1}) exceeds the hydrogen bond dissociation thresholds (Suslick, 1990).

Despite these benefits, US pretreatment can sometimes reduce esterification efficiency. Liu et al. (2008) pretreated sugarcane bagasse in pyridine at 30 °C using US at 40 kHz for 50 min, resulting in a 15 % decrease in ester yield compared to non-pretreated biomass, which was attributed to a reduction in molecular weight. US enhanced esterification in ionic liquids as Ma et al. (2012) reported an 82 % *DS* increase when extending US treatment from 20 to 120 min during cellulose esterification with glutaric anhydride in 1-butyl-3-methylimidazolium chloride ([Bmim]Cl) at 40 kHz and 85 °C. Similarly, *DS* increased by 46 % compared to silent conditions with phthalic anhydride in [Bmim]Cl at 105 °C, US at 40 kHz for 60 min, (Ma et al., 2013).

An US bath operating at 40 kHz and 35 °C was adopted to esterify MCC, in DMAc with DMAP, EDCHCl and oleic acid as *EA* (Hou et al., 2023). DMAP acted the catalyst, and EDCHCl as the dehydrating agent to convert oleic acid into anhydride. They obtained the highest *DS* of 1.55 in DMAc after 6 h of reaction, a molar ratio oleic acid/MCC of 6:1 and a US intensity of 300 W m^{-2}. US improved reactivity by enhancing cellulose dissolution, exposing hydroxyl groups, and breaking fiber aggregates, leading to a homogeneous reaction medium that promotes the reaction with oleic acid (Hou et al., 2023).

The present research explores the esterification of cellulose with long chain FFA (oleic acid and stearic acid) to make cellulose thermoplastics, enhanced by US, representing a combination not previously investigated in the literature. Unlike earlier studies, this work integrates the approaches just mentioned to achieve reduced reaction time, lower consumption of possibly harmful chemicals and decreased energy requirements for producing thermoplastic materials or oligomers from cotton linters and cellulose fibers. Long chain FFA were selected as they act as an internal plasticizer. Additionally, COMSOL Multiphysics simulated the US activity – acoustic pressure, active cavitation volume

Table 1
Design of experiments.

#	Experiment	Cellulose	*EA*	*EA*/cellulose (mol^{-1})	Temperature (°C)	Time (h)	*P* (W)	*PD* (W L^{-1})	*DS*
1	C100	1	Oleoyl chloride	6	100	1	-	-	2.62 ± 0.40
2	C40	1	Oleic Acid	6	40	24	–	-	0.87 ± 0.15
3	C60	1	Oleic Acid	6	60	24	–	-	0.61 ± 0.11
4	C80	1	Oleic Acid	6	80	24	–	-	1.44 ± 0.25
5	C80_2	2	Oleic Acid	6	80	24	–	-	0.37 ± 0.06
6	C80_S	1	Stearic Acid	6	80	24	–	-	0.13 ± 0.02
7	C80_3	1	Oleic Acid	3	80	24	–	-	0.33 ± 0.06
8	U40_1_4	1	Oleic Acid	6	40	0.5	4.39	409	0.21 ± 0.04
9	U60_1_4	1	Oleic Acid	6	60	0.5	4.39	409	0.14 ± 0.02
10	U80_1_4	1	Oleic Acid	6	80	0.5	4.39	409	0.14 ± 0.02
11	U40_2_5	1	Oleic Acid	6	40	0.5	6.70	624	0.17 ± 0.03
12	U40_3_6	1	Oleic Acid	6	40	0.5	9.01	839	0.029 ± 0.005
13	U40_1_2	1	Oleic Acid	6	40	0.5	4.39	204	0.15 ± 0.02
14	U40_1_1	1	Oleic Acid	6	40	0.5	4.39	136	0.18 ± 0.03
15	U20_1_1	1	Oleic Acid	6	20	0.5	4.39	136	0.38 ± 0.06
16	U20_2_2	1	Oleic Acid	6	20	0.5	6.70	208	0.32 ± 0.05
17	U20_3_3	1	Oleic Acid	6	20	0.5	9.01	280	0.30 ± 0.05
18	U40_1_1	1	Oleic Acid	6	40	0.5	4.39	136	0.59 ± 0.11
19	U60_1_1	1	Oleic Acid	6	60	0.5	4.39	136	0.67 ± 0.03
20	U80_1_1	1	Oleic Acid	6	80	0.5	4.39	136	0.48 ± 0.02
21	U40_2_2	1	Oleic Acid	6	40	0.5	6.70	208	0.74 ± 0.03
22	U40_3_3	1	Oleic Acid	6	40	0.5	9.01	280	0.42 ± 0.02
23	U40_1_2	1	Oleic Acid	6	40	0.5	4.39	204	0.30 ± 0.01
24	U20_1_1	1	Oleic Acid	6	20	0.5	4.39	136	1.79 ± 0.03
25	U20_2_2	1	Oleic Acid	6	20	0.5	6.70	208	1.58 ± 0.04
26	U20_3_3	1	Oleic Acid	6	20	0.5	9.01	280	1.20 ± 0.10

The first experiment (#1) corresponds to the experiment in pyridine with oleoyl chloride. The second part of the table (experiments #2-#7) corresponds to the DoE of conventionally stirred esterification (silent conditions). The third part (experiments #8-#17) corresponds to the DoE of US-assisted esterification with DS determined by ^{1}H NMR as a response. The fourth part (experiments #18-#26) corresponds to the DoE of US-assisted esterification with DS determined by gravimetric analysis as a response.

and acoustic streaming velocity – to understand the phenomena occurring within the reactor. The proposed process offers a promising way for the conversion of renewable feedstocks into biodegradable and potentially compostable thermoplastic materials or depolymerized cellulose esters with biomass-derived FFA, an area documented in a limited extent.

2. Material and methods

2.1. Materials

All chemicals were used as received, i.e. N,N-dimethylacetamide (DMAc, 99 %, Thermoscientific), lithium chloride (LiCl, 99 %, Sigma), p-toluenesulfonyl chloride (p-Tos, 98 %, Thermoscientific), pyridine (99 %, Sigma) oleic acid (90 %, Aldrich), stearic acid (Anachemia), oleoyl chloride (89 %, Sigma), anhydrous ethanol (Commercial Alcohols).

This study included two sources of cellulose: cotton linters cellulose (C1, DP = 138, Sigma), and cellulose fibers (C2, DP = 926, Recyc php). This latter is recycled from used diapers by Recyc php.

2.2. Esterification of cellulose

The esterification consisted of the following steps, including dissolution: 10 mL of DMAc at 130 °C were added to activate 0.25 g of cellulose for 2 h at 1150 rpm, 0.75 g of LiCl were added (Heinze, 2015)). When the cellulose is fully dissolved and the mixture is transparent, p-Tos and oleic acid were added with a *EA*/cellulose/p-Tos of 1:6:6 molar ratio (Fig. 1). Further reaction details are found in the Supplementary information (SI).

Three designs of experiments (DoE) were built, applying a fractional factorial layout to all. The first one included six experiments, the second ten, and the third nine. The first DoE aimed to confirm the effect of the molar ratio of *EA*/cellulose, temperature, cellulose source and FFA (saturated or not) on the esterification of cotton cellulose without US. The independent variables are:

- Molar ratio of *EA*/cellulose, 3 and 6;
- Temperature, 40 °C, 60 °C and 80 °C;
- Cellulose, C1 and C2;
- FFA, oleic acid and stearic acid.

The second and third DoE investigated the US-assisted esterification of C1 with oleic acid, where the independent variables are:

- Temperature, 20 °C, 40 °C, 60 °C and 80 °C;
- US power (*P*), 4.39 W, 6.70 W and 9.01 W;
- Total reaction volume (*v*), 32.2 mL, 21.5 mL and 10.7 mL.

The response variables are the *DS* determined by ^{1}H NMR-HRMAS spectroscopy for the conventional esterification and by gravimetric analysis for the US-assisted esterification (for US-assisted esterification exclusively as it provided a larger sample set and enabled a more reliable comparison with *DS* by ^{1}H NMR analysis). For the sample obtained with oleoyl chloride in pyridine (Table 1), the *DS* was determined by ^{1}H NMR analysis. Table 1 lists all the experiments and operating conditions. Gravimetric analysis tends to overestimate the *DS* because it cannot differentiate substitution from residual solvents and FFA or reaction by-products. It is emphasized as the esterification agent is a long-chain FFA like oleic acid, which persist into the cellulose structure after purification (Heinze et al., 2018). ^{1}H NMR analysis provides a more selective determination of the *DS*. It distinguishes substituted and unsubstituted cellulose groups (Habibi, 2014). However it has limitations such as flawed *DS* determination in case of inadequate preparation (Abdul Hadi et al., 2020), or limited sample solubility and poor resolution in case of low *DS* (Ferro et al., 2017).

Statistical analysis identified significant dependent variables and the relationship within the data. Initially a predictor screening analysis with Bootstrap forest partitioning, identified the dependent variables contributing the most variance to the response variables. Then, the non-significant variables were eliminated to develop a linear regression model that predicted the response variables with a 95 % confidence

interval (CI) accuracy. The actual vs predicted responses were plotted, where the actual refers to the *DS* obtained experimentally, whereas predicted refers to the *DS* determined by the prediction regression.

The labeling of the sample names is detailed as follows, with all parameters provided in Table 1. The reference parameters for sample preparation involve using cellulose C1 and oleic acid as the *EA*, with an *EA*/cellulose ratio of 6. Samples prepared without US are labeled as C#, while those prepared with US are labeled as U#. The first number in the label represents the esterification temperature, ranging from 20 °C to 100 °C. For samples prepared under silent conditions (without US), the second identifier denotes specific parameters. C80_2 was prepared using cellulose C2, C80_3 used a *EA*/cellulose ratio of 3:1, and C80_S used stearic acid as the *EA* instead of oleic acid.

C100 serves as a reference material, produced at 100 °C using oleoyl chloride as the *EA*.

For US-assisted esterification, the second digit in the label corresponds to the *P*, ranging from 1 (4.39 W) to 3 (9.01 W). The third digit indicates the power density (*PD*), ranging from 1 (139 W L^{-1}) to 6 (839 W L^{-1}). For example, U20_1_1 was prepared at 20 °C, with a *P* of 4.39 W and a *PD* of 139 W L^{-1}. In Table 1, the mentioned power is the US power delivered to the reaction medium, calculated by calorimetric calibration (Li et al., 2020).

2.3. FTIR attenuated total reflection (ATR) analysis

The functional groups of ester samples were identified by a Perkin Elmer Spectrum 65 Fourier-transform infrared (FTIR) spectrometer with an attenuated total reflectance Miracle ATR accessory. 32 scans were used, with a resolution of 2 cm^{-1} from 4000 cm^{-1} to 600 cm^{-1}.

2.4. Determination of the DS

The *DS* was determined after high-resolution magic angle spinning (HRMAS) ^{1}H NMR in dimethylsulfoxide (DMSO) with sodium trimethylsilylpropanesulfonate (DSS) as a standard. The equipment was a Bruker AVANCE II operating at 400 MHz with a probe cross polarization magic angle spinning (CPMAS). The procedure is described in Section S3.

For these calculations, it is assumed that the molecular weight of the oleic acid chain was assumed at 265.5 g mol^{-1} by considering that during esterification a hydroxyl group is converted into ester. All the oleic acid in each sample was grafted onto the cellulose chains, which is confirmed by FTIR spectra (Fig. 3).

Additionally, the *DS* was verified by gravimetric analysis. After drying and weighing cellulose esters samples, the *DS* was calculated with the following equation:

$$DS = \frac{m_1 - m_0}{(M-1)\cdot n_0} \quad (1)$$

where m_1 is the weight of the ester's sample, m_0 is the weight of unmodified cellulose, n_0 is the number of moles of unmodified cellulose, M is the molecular weight of an oleoyl group ($M = 265.5$ g mol^{-1}), and 162 is the molecular weight of AGU in g mol^{-1}.

2.5. X-ray diffraction (XRD)

A Bruker D8 Advance diffractometer was employed to scan unmodified cellulose, sample U20_1_1 (lowest power density and temperature, highest *DS*) and sample U80_1_1 (highest temperature) from 2° to 50° of 2θ. It is essential to determine whether esterification preserves or disrupts the cellulose structure.

2.6. Thermal behavior

Prior to differential scanning calorimetry (DSC), a TA Instruments thermogravimetric analyzer (TGA) Q500 was used to determine the weight loss of the sample C80, which had the highest *DS* after conventional esterification. The sample was heated from 25 °C to 500 °C at 10 °C min^{-1} under a 40 mL min^{-1} nitrogen flow.

The transition temperatures of the ester samples were determined with a TA Instruments calorimeter Q200 with an RSC 90 cooling system using a heating ramp from −70 °C to 180 °C at 20 °C min^{-1} and with a nitrogen flow of 50 mL min^{-1}. The sample weight was around 3 mg. This analysis is essential to reveal the glass transition and melting temperatures of the esters to identify operating temperatures for further processing.

Table 2
Properties of cellulose esters solutions at 20 °C.

Cellulose concentration, g L^{-1}	Speed of sound, m s^{-1}	Density, kg m^{-3}	Viscosity, Pa·s
25	1495.8	936.2	$23.3{\cdot}10^{-3}$

2.7. Viscosity and density measurements

The numerical simulations aimed to calculate the minimum acoustic pressure (p_{min}), maximum acoustic pressure (p_{max}), cavitation zones volume (V) and acoustic streaming velocity (u) in cellulose esters solution at 25 g L^{-1}. The fluid was approximated to Newtonian, and its density (ρ) and viscosity (μ) were measured as data to feed to COMSOL Multiphysics. ρ and μ were measured at various temperatures, after 2 h of cellulose esterification at 25 g L^{-1}.

An Anton Paar DMA 4500 density meter instrument was used to determine ρ. μ was measure with a Thermo Scientific Haake Viscotester iQ. The rheometer has a coaxial cylinder configuration and holds 3 mL samples. The ramp was: 120 s at a shear rate of 1 s^{-1}, followed by an increase in the shear rate to 500 s^{-1}.

2.8. Speed of sound measurements

The speed of sound (c) in cellulose ester solutions was measured using an Olympus V306 immersion transducer. The transducer's active element has a diameter of 13 mm. Operating at a frequency of 2.25 MHz, the transducer transmitted signals through a polystyrene container holding 50 mL of the cellulose ester solution. It was affixed to the container's side, and the solution was introduced using a pipette to minimize movement during filling and emptying, ensuring the acoustic waves propagated perpendicularly to the opposite container wall. The transducer was connected to an Agilent Technologies 33220A 20 MHz waveform generator and a GW Instek GDS-1000A-U Series oscilloscope for monitoring.

Initially, a signal was transmitted through deionized water to measure the round-trip distance of the sound wave within the fluid. It was assumed that the wave propagated solely through the water, with a speed of 1498 m s^{-1}, since it was not feasible to determine the thickness of the gel and the polystyrene wall. The wave covered a total distance of 44.67 mm. Seven measurements of the sound speed were taken via the oscilloscope, and an average value was calculated. These results were subsequently input into COMSOL Multiphysics (Table 2).

This assumption that the wave traveled exclusively through the liquid underestimated the actual speed of sound. In reality, the speed of sound in polystyrene is approximately twice that in water, oils, or ethanol (Olympus, n.d.), which overestimated the attenuation of the sound waves in the solutions.

3. Mathematical model and simulation

COMSOL Multiphysics 6.1 solved the Helmholtz equation, a steady state form of the wave equation, to determine p_{min} and p_{max} in the sonoreactor (Fig. 2). To determine V, the acoustic pressure above the

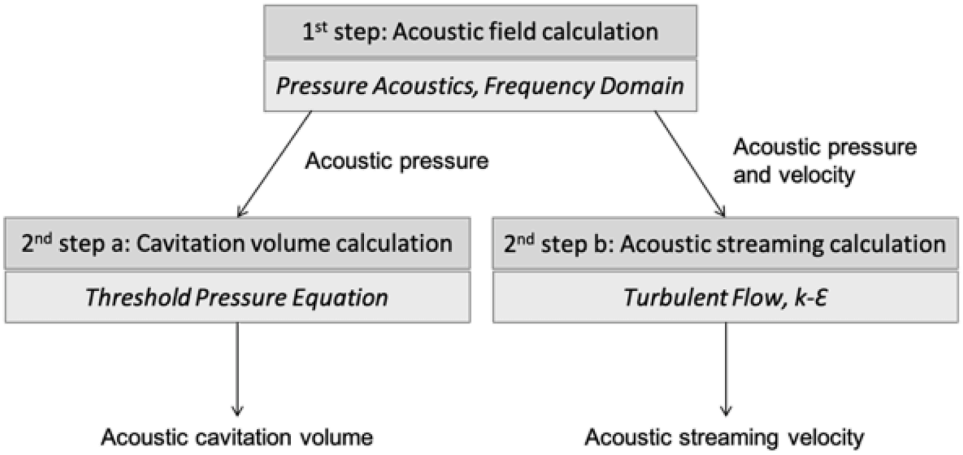

Fig. 2. Simulation steps for acoustic pressure, cavitation volume and acoustic streaming velocity determination.

cavitation pressure threshold was considered (Fig. 2). The turbulent flow module calculated *u*, solving the Navier-Stokes equation (Fig. 2).

It is assumed that the fluid is incompressible and Newtonian, the sound waves exhibit linear behavior, and the shear stress could be neglected. The bubble to liquid volume ratio is low so the system is computed as a single-phase fluid (Commander and Prosperetti, 1989). The properties of the sonicated fluid are independent of the temperature and bubble volume fraction.

US waves reflect with a deviation of acoustic impedance (*Z*). *Z* is product of the material's density and speed of sound. The following boundary conditions were applied:

1. At the boundary liquid-glass, $Z = 2230$ kg m^{-3}·5640 m s^{-1}, for steps 1 and 2a. For step 2b, we applied a no-slip boundary condition.
2. At the boundary liquid-air $Z = 1.2$ kg m^{-3}·343 m s^{-1}, for steps 1 and 2a. For step 2b, we applied a pressure outlet, with a pressure of 0 Pa.
3. At the boundary liquid-probe $Z = 4470$ kg m^{-3}·4987 m s^{-1}, for steps 1 and 2a. For step 2b, we applied a slip boundary condition.
4. At the tip of the probe, a pressure amplitude p_a was set for steps 1 and 2a.

Section S4 details, the equations solved during the simulations, the assumptions, the geometry, the boundary conditions (Figure S2) and the mesh of the model (Goris et al., 2025; Joyce Tiong et al., 2025; Schieppati et al., 2024).

The independent variables for these simulations are:

- *P*, 4.39 W, 6.70 W and 9.01 W;
- *v*, 32.2 mL, 21.5 mL and 10.7 mL;
- Temperature, 20 °C, 40 °C, 60 °C and 80 °C;

The response variables are p_{min}, p_{max}, *V* and *u*. A statistical analysis identified significant dependent variables and relationship within the data, as in Section 2.2.

4. Results and discussion

4.1. Cellulose sources and fatty acids effects

Before conducting US-assisted esterification, the use of long chain FFA was investigated instead of acyl chlorides and anhydrides to produce cellulose esters, aiming for safer, less expensive and biomass-derived *EA*. During the synthesis process, the influence of parameters such as the *EA*/cellulose ratio, the source of cellulose, and the type of

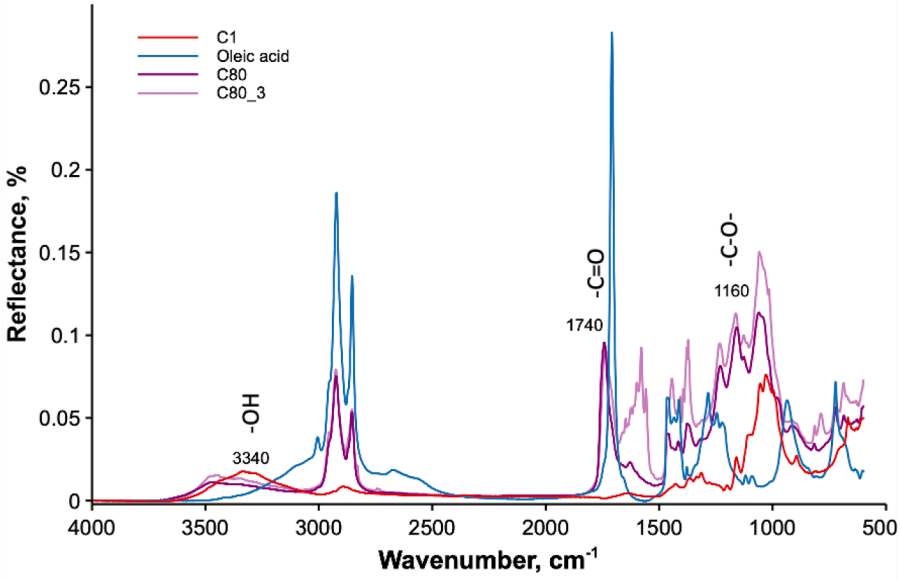

Fig. 3. FTIR spectra of the unmodified cellulose C1, unmodified oleic acid and cellulose esters produced with various *EA*/cellulose ratios, 6:1 and 3:1.

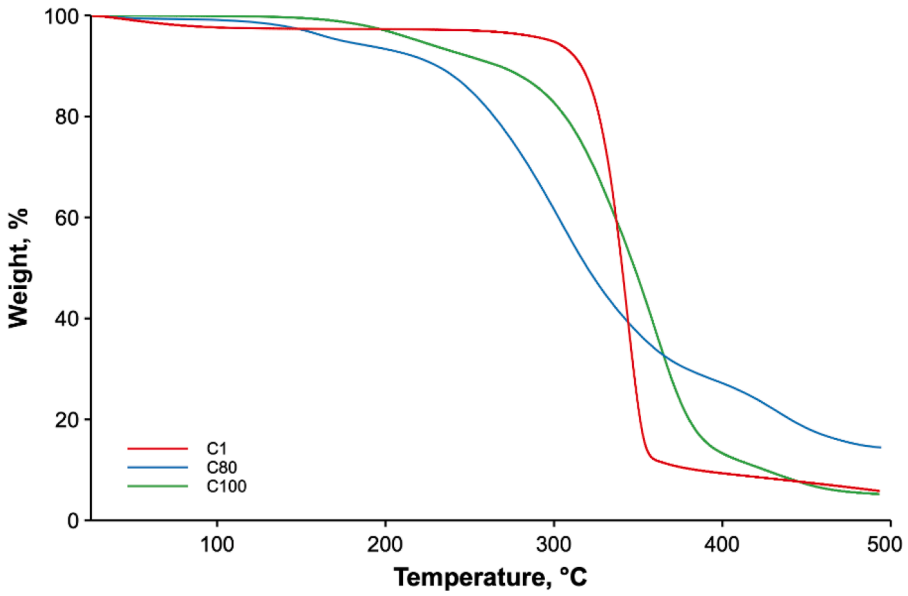

Fig. 4. Weight loss of unmodified cellulose (C1) and esters treated at two different temperatures (C80 and C100) and exhibiting the best DS.

FFA, was investigated on the *DS*. The results are presented in Table 1. The *DS* was five times higher, with oleic acid at a molar ratio p-Tos/*EA*/cellulose of 6:6:1 compared to 3:3:1 (1.44 against 0.33). Hou et al. (2023) observed the same trend due to an increased frequency of interactions between the OH groups of cellulose and the *EA*. Regarding the nature of *EA*, the use of stearic acid resulted in lower *DS* than oleic acid, with a *DS* of 0.13 against 1.44, respectively. In our case, the chain length remains unchanged, but the degree of saturation differs, with only one C=C unsaturation on the oleic acid chain. Crépy et al. (2009) produced cellulose stearate with a *DS* of 2.3 and cellulose oleate with a *DS* of 2.9. They mentioned that the unsaturation facilitates the reaction, but gave no further details. The double bond in oleic acid restricts chain mobility, but its *cis*-configuration makes it less thermodynamically stable than stearic acid, and thus more reactive (Rustan and Drevon, 2005). The double bond in the alkyl chain increases the electron density, making the carboxylic group of oleic acid more reactive toward attack from the hydroxyl group of cellulose than the carboxylic group of stearic acid. The unsaturation also reduces Van der Waals interactions among the oleic acid molecules, which increases the diffusion of oleic acid and reduces its melting point, increasing the contact with cellulose hydroxyl groups. The reduced Van der Waals interactions among the oleic acid molecules also decreases the viscosity of the reaction medium, facilitating the mixing (Heinze et al., 2018).

Esters from two different sources of cellulose were synthetized, C1 with a DP of 138, and C2 with a DP of 926 (Figure S1). C1 and C2's esters had a *DS* of 1.44 and 0.37, respectively. Similarly, Willberg-Keyriläinen et al. (2016) and Uschanov et al. (2011) observed that reduction in cellulose molecular weight increased with the *DS* of esters produced. Willberg-Keyriläinen et al. (2016) increased the *DS* by a factor of 3 when molecular weights decreased from 520 kg mol^{-1} to 80 kg mol^{-1}. They explained it by the increased accessibility of the cellulose surface for reaction.

In this study, the degree of substitution (DS) increases with the EA/cellulose ratio when using C1 and decreases when using C2. The DS also

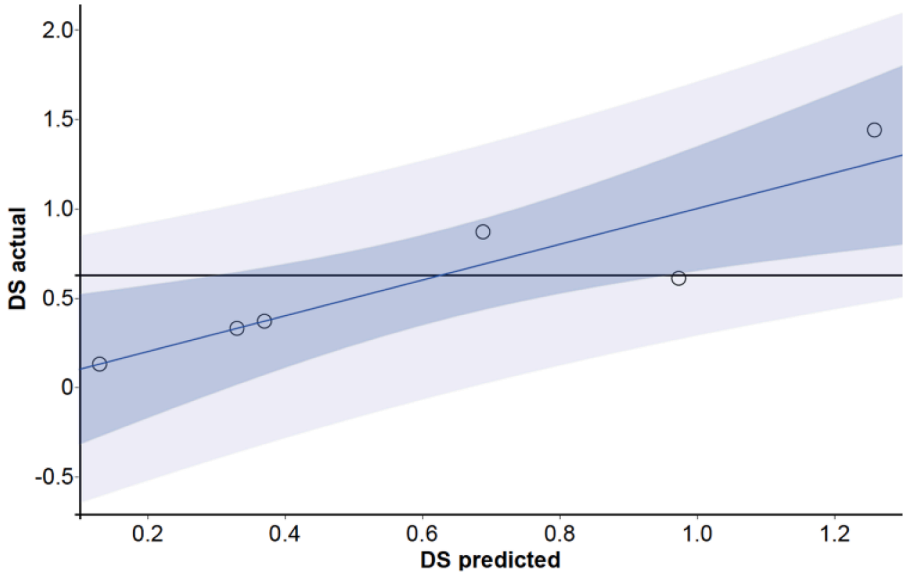

Fig. 5. Actual vs. predicted DS (○) determined by ^{1}H NMR for esters produced with conventional conditions. – Regression, ■ 95 % CI of prediction, RMSE = 0.445, R^2 = 0.823, p-value = 0.0125, – Mean of response (0.625), ■ Prediction interval.

Table 3
Predictor screening analysis of *DS* determined by ^{1}H NMR for esters produced with conventional conditions.

Predictor	Portion*
Temperature	31.6 %
EA	30.8 %
EA/Cellulose	23.1 %
Cellulose	14.5 %

* Portion of the variance from the prediction.

increases with oleic acid and decreases with stearic acid. A possible explanation for the low *DS* obtained could be the precipitation of solid, forming heterogeneous phase, as noticed during the esterification reaction. This affects the mixing efficiency, as the reaction mixture had a stationary solid layer on top and a lower liquid layer (Barthel and Heinze, 2006).

The comparison of FTIR spectra of cellulose, FFA, and esters samples show the progress of esterification and the impact of our different steps used for washing and extraction. Following a rigorous washing and extraction method, all samples do not exhibit any traces of solvent nor FFA (Fig. 3). Esters samples (C80 and C80_3) have characteristic peaks at 1740 cm^{-1} and 1150–1160 cm^{-1} (Fig. 3), which correspond to the vibration of C=O and C—O from ester groups, respectively, confirming the formation of ester bonds onto the cellulose backbone. This observation is supported by a decrease in the intensity of the peak at around 3340 cm^{-1}, characteristic of -OH groups, shifting towards higher wavenumber (Fig. 3). This suggests the substitution of hydroxyl groups into esters (Duchatel-Crépy et al., 2020), reducing hydrogen bonding and enabling the dissolution of cellulose (Lindman et al., 2010; Wang et al., 2012).

In the TGA, the degradation took place in two stages for C1 and in three stages for C100 and C80 (Fig. 4). The initial weight loss is attributed to the evaporation of adsorbed water (Jandura et al., 2000b). Esters samples started to decompose at lower temperatures (210 °C for C100, and 170 °C for C80) compared to unmodified cellulose (295 °C), as reported by Costa et al. (2023). Grafting long chains FFA to cellulose decreased the materials crystallinity, which lowers decomposition temperature of cellulose derivatives (Jandura et al., 2000b). The lower decomposition temperature of cellulose esters also occurs due to the fact that FFAs alone have a lower decomposition temperature than cellulose (Uschanov et al., 2011).

The primary degradation step of unmodified cellulose occurs at 340 °C, resulting in the breakdown of cellulose into carbon dioxide and water. In contrast, for cellulose esters (358 °C for C100 and 300 °C for C80), this step involves the degradation of the cellulose backbone, ester groups, and unsaturated bonds of oleic chains. The third degradation step of esters corresponds to the decomposition of oleic acid alkyl chains into volatiles (Hou et al., 2023). This step results from the crosslinking and crystallization of aliphatic chains of saturated free fatty acids (FFA) into ordered structures during heating. Jandura et al. (2000b) observed this last degradation in the range of 300 °C to 400 °C for oleic acid cellulose esters with a DS as low as 0.08.

4.2. Effect of temperature

The reaction temperature affects both the conventional and the US-assisted processes. In conventional esterification, the *DS* increases by 66 % from 40 °C to 80 °C. For the DoE of conventional esterification, the regression (Fig. 5) resulted in the following equation:

$$DS = -0.499 + 0.285\cdot\frac{T-60}{20} + 0.464\cdot\frac{\frac{EA}{C}-4.5}{1.5} + C\cdot\begin{pmatrix}1\rightarrow 0.444\\ 2\rightarrow -0.444\end{pmatrix} + EA\cdot\begin{pmatrix}\mathrm{Ol}\rightarrow 0.564\\ \mathrm{St}\rightarrow -0.564\end{pmatrix} \quad (2)$$

All dependent variables have a significant effect on the *DS*, accounting for a percentage of the variance on the same order of magnitude (Table 3). The DS increases with temperature (T) (Eq. (2)).

Lease et al. (2021) reported a similar behavior with *DS* increasing nearly 200 fold when the temperature was raised from 50 °C to 100 °C. Jebrane et al. (2017) quantified esterification by measuring the intensity of the FTIR peak corresponding to the C=O vibration, which increased from 0.2 to 0.6 as the temperature rose from 90 °C to 125 °C, confirming the increase in *DS*. Mikkola et al. (2007) also reported an increase in the *DS* from 0.01 at 60 °C to 0.31 at 100 °C.

The peaks at 2920 cm^{-1} and 2850 cm^{-1} (Fig. 6) are characteristic of the CH_2 stretching of alkyl chains from FFA. The unsaturation of oleic acid is indicated by the peaks at 3005 cm^{-1} (C—H stretching) and 1630 cm^{-1} (C=C stretching), respectively. Additionally, the peak at 1460 cm^{-1} is characteristic of C—H scissoring in CH_2 and CH_3 (Jebrane et al., 2017), and the peak at 920 cm^{-1} corresponds to the C—H bending of -CH=CH- groups (Jandura et al. (2000a)). The carbonyl stretch vibration (C—O) is observed at 1235 cm^{-1} (Liang et al., 2013). Peaks at 720 cm^{-1} are

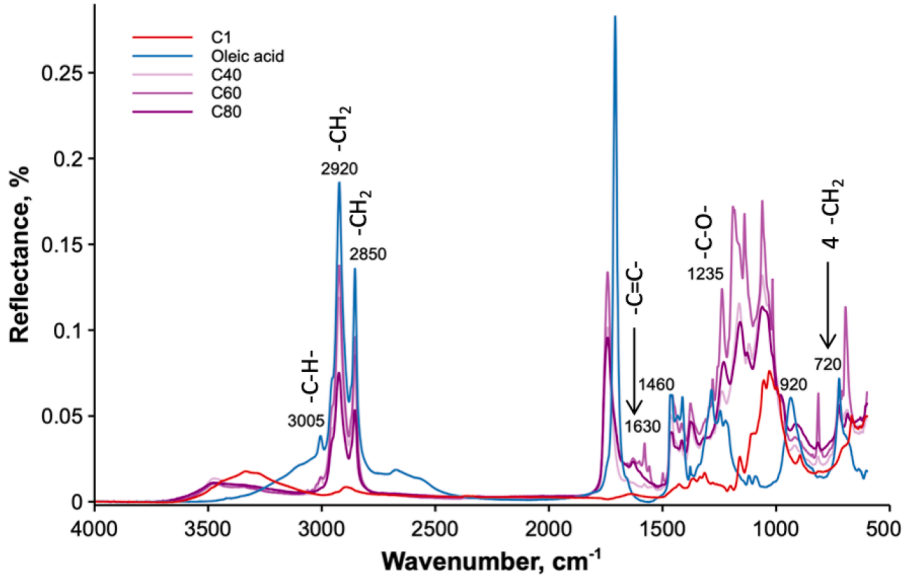

Fig. 6. FTIR spectra of reference cellulose C1, oleic acid and cellulose esters produced at various temperatures.

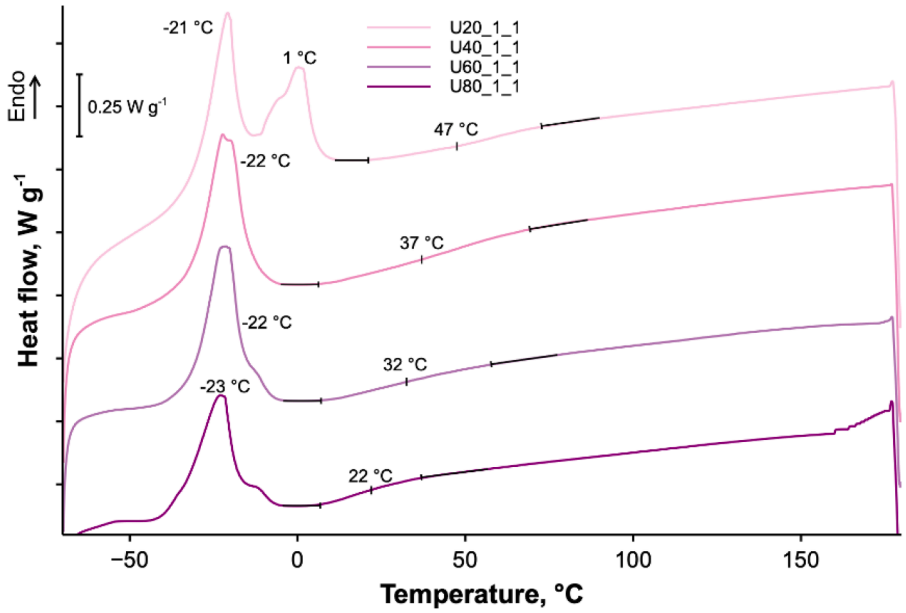

Fig. 7. DSC curves of cellulose esters produced with US at 136 W L^{-1} and various temperatures.

characteristic of at least four CH_2 groups linked (Duchatel-Crépy et al., 2020). These peaks are present in all our samples spectra, however, they alone do not confirm esterification, as they could be attributed to unreacted FFA. Thus, the *DS* was determined by gravimetric and ^1H NMR analyses.

Regarding samples prepared with US (with *DS* determined by gravimetric analysis) at a fixed *PD* of 136 W L^{-1}, an increase in reaction temperature from 20 °C to 80 °C resulted in a decrease in the *DS* from 1.79 to 0.48 (Table 1). However, Ma et al. (2013, 2012) showed the opposite trend by reporting that the increase of reaction temperature from 70 °C to 95 °C increased the *DS* by 124 % (with glutaric anhydride), and from 95 °C to 120 °C increased the *DS* by 48 % (with phthalic anhydride). They attributed it to enhanced reaction rate with better diffusion of *EA* in the reaction media. The decrease of *DS* is attributed to the possible generation of H• and •OH radicals from the dissociation of water (formed during esterification) inside cavitation bubbles. These radicals can cleave the glycosidic bonds of cellulose or the ester links, decreasing the *DS* (Haouache et al., 2020).

At a fixed cellulose concentration, the increase in temperature affects the reaction mixture's properties, such as μ and ρ, which in turn influences acoustic cavitation. From 20 °C to 80 °C, μ dropped by 75 %, and ρ by 4 %. Simulation results show that the increase of the reaction temperature from 20 °C to 80 °C at 25 g L^{-1}, is independent of p_{max}, p_{min} and u. However, it increases V by almost 10 times for a reaction volume of 32.2 mL. A predictor screening of V determined that, in a reaction volume of 32.2 mL, μ explains 57 % of the variance. Viscosity affects the acoustic attenuation, as more viscous liquids are prone to fewer shock waves and release less energy during cavitation, hence smaller V. This corroborates the abovementioned hypothesis about the decrease of *DS* with increasing temperature.

The thermal transitions of cellulose esters produced at different temperatures without US are presented in Figure S3. Similarly to the starting material C1, C80, C60 and C40 have a T_g close to 5 °C. Pure oleic acid undergoes a polymorphic transformation with a transition from γ to

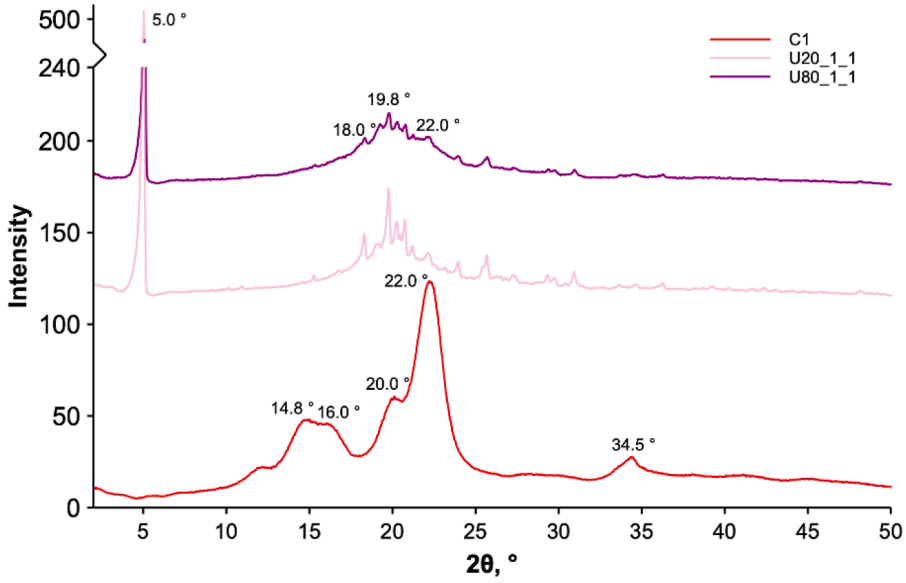

Fig. 8. XRD diffractogram of unmodified cellulose (C1), and esters treated at two different temperatures (U20_1_1 and U80_1_1).

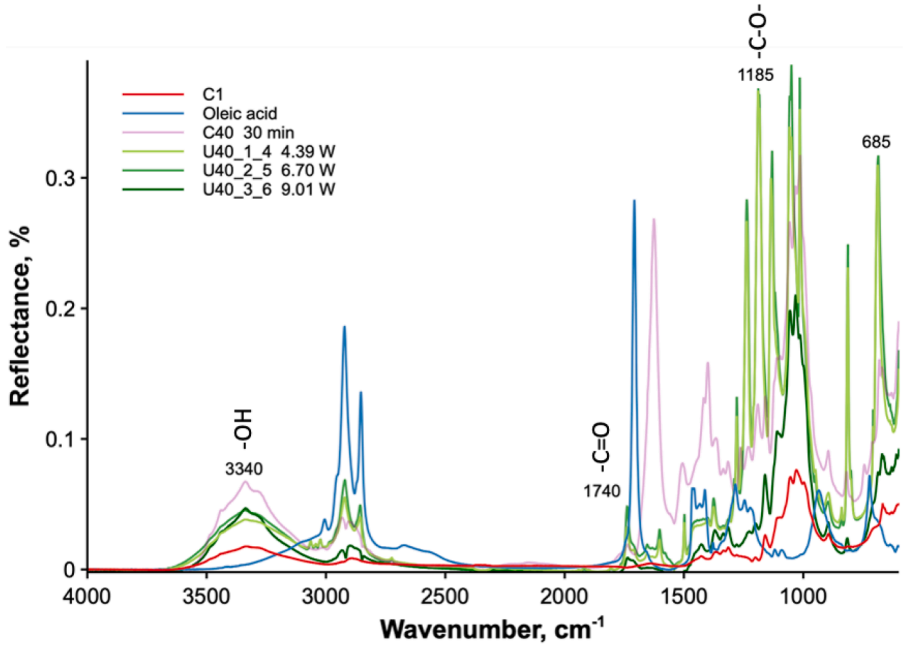

Fig. 9. FTIR spectra of cellulose esters produced at different ultrasonic powers, and esters produced in silent conditions after 30 min.

α-form at −16 °C, followed by α-form melting at 13 °C (García-Zapateiro et al., 2013). The thermal behavior of the cellulose esters synthesized with US at a *PD* of 136 W L^{-1} and at four different temperatures is presented in Fig. 7. The *DS* for US-produced cellulose esters varies with reaction temperatures, reaching 1.79 at 20 °C, 0.59 at 40 °C, 0.67 at 60 °C, and 0.48 at 80 °C (Table 1). A melting endotherm linked to alkyl side chains of FFA occurs around −20 °C, with the melting temperature (T_m) decreasing from −21 °C to −23 °C as reaction temperature increases. From 40 to 80 °C, the low *DS* suggests that the alkyl side chains are more mobile and less densely packed, resulting in a decrease in T_m. This results in a single broad melting peak with a slight shoulder at around −10 °C, that indicates limited polymorphism (Morselli Ribeiro et al., 2012). However, at 20 °C, the higher *DS* hints at tightly packed alkyl chains. The melting region for the US-prepared ester exhibits two distinct melting endotherms at −21 °C and 1 °C suggesting the presence of different crystal domains (Sealey et al., 1996).

This is reflected as well with the increase in T_g from 22 °C to 47 °C as the *DS* increases from 0.48 to 1.79 (Fig. 7). This is attributed to the increase of steric hindrance which increases the stiffness of the cellulose chains as more FFA are grafted onto cellulose backbone (Sealey et al., 1996). However, it is not always the case. Depending on the structure and length of the chain, a decrease of T_g was observed with increased *DS* and was interpreted as a plasticizing effect of the long chain FFA (Duchatel-Crépy et al., 2020; Tanaka et al., 2017).

The T_g of cellulose esters increases with increasing DP, because the chains begin to entangle, limiting their mobility (Tarasova et al., 2024). Thus, it is suggested that the T_g obtained are lower than those mentioned in the literature due to the depolymerization of cellulose chains, which decreases the DP.

Alteration of the crystalline structure of cellulose due to dissolution, sonication and esterification is also confirmed by the decrease of intensity of crystalline reflexes (Fig. 8). Unmodified cellulose (C1) shows peaks of cellulose Iβ: 14.8°, 16.0°, 20.0°, 22.0°, 34.5°, corresponding respectively to crystals planes 101, 110, 021, 200, 004 (Jandura et al., 2000a). Ester cellulose produced with US at 20 and 80 °C exhibit a decrease in crystalline peak intensity and form amorphous peaks at 18° and 19.8° Moreover, a new peak at 5.0° in the diffractogram of ester celluloses, confirms the crystallization of grafted fatty chains (Sejati et al., 2023), with its intensity increasing with the *DS*.

4.3. Comparison of esterification under sonication and silent condition

The effect of process intensification compared to the conventional method (silent conditions) on esterification was investigated with different *P* ranging from 4.39 W to 9.01 W, in a fixed volume of 10.7 mL. After US-assisted esterification, sharp peaks are observed at 1740 cm^{-1} and 1185 cm^{-1}, characteristic of C=O and C—O esters bond stretching (Fig. 9). At 9.01 W (sample U40_3_6), both peaks have lower intensities, which suggests a small degree of esterification (Fig. 9).

Our US-produced cellulose esters exhibit intense hydroxyl peaks at 3340 cm^{-1} and 685 cm^{-1}, characteristics of OH covalent bonds and C—OH groups, respectively. These peaks are more pronounced compared to silent conditions, which reflect low level of oleic acid substitution (Fig. 9). The FTIR results are in accordance with the change in *DS* measured by ^{1}H NMR analysis. As the increase of *P* from 0 W to 4.39 W (3.31 W cm^{-2}) to 9.01 W (6.79 W cm^{-2}), the *DS* dramatically decrease from 0.87 to 0.21 to 0.029 (Fig. 10a), respectively. However, it is noteworthy that under US, cellulose was esterified within only 30 min against 24 h under conventional heating and stirring. This partial esterification of the cellulose surface results from insufficient amount of energy supplied to the reaction mixture and/or time. A 24 h US-assisted esterification was not performed due to the erosion of US probe and the excess energy supplied, which would negate the benefits of intensification, and degrade cellulose. Additionally, the *DS* was also determined at 40 °C by gravimetric analysis. As *P* increased from 0 W to 4.39 W, so did the *DS* from 0.33 (predicted by Eq. (4)) to 0.59. A further increase of *P* to 9.01 W decreased the *DS* to 0.42, with a peak of 0.74 at 6.70 W (Fig. 10b).

At 80 °C, the increase in *P* from 0 W to 4.39 W, decreased the *DS* from 1.44 to 0.14. A further increase of *P* to 9.01 W increased the *DS* to 0.87 (predicted by Eq. (3)). The maximum *DS* was obtained at 20 °C, indeed, the *DS* increased from 1.29 at 0 W (predicted by Eq. (4)) to 1.79 at 4.39 W (the peak), than decreased to 1.20 at 9.01 W (Fig. 10b).

The *DS* of US-produced ester determined by ^{1}H NMR analysis, resulted in the regression in Fig. 11 and the following equation:

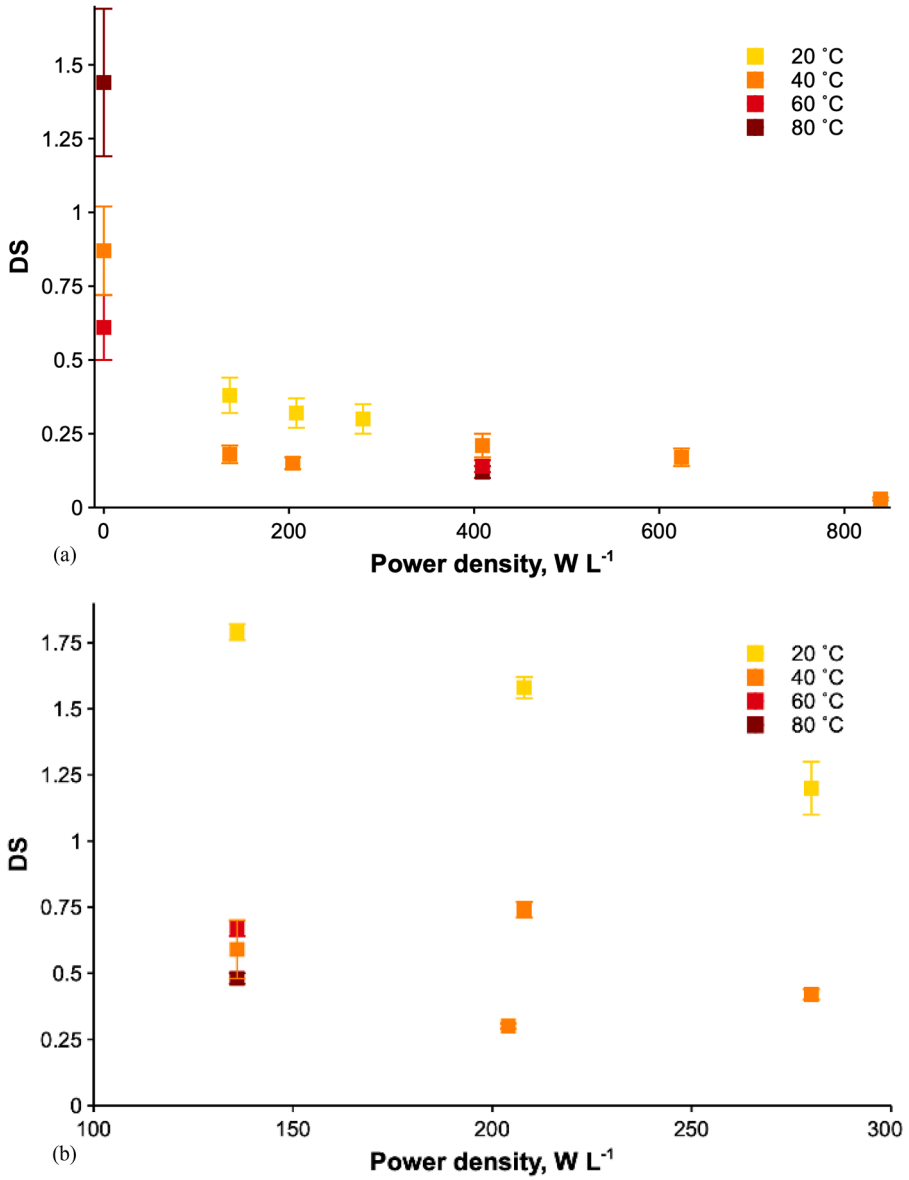

Fig. 10. DS determined by (a) ^{1}H NMR and (b) gravimetric analysis vs. power density at various temperatures.

$$DS = -0.335 + 6.43{\cdot}10^{-2}{\cdot}P + 4.96{\cdot}10^{-4}{\cdot}PD + 3.80{\cdot}10^{-2}{\cdot}\left(\frac{T-60}{20}\right) (P-5.78) + 6.30{\cdot}10^{-4}{\cdot}\left(\frac{T-60}{20}\right)(PD-365) -1.37{\cdot}10^{-4}{\cdot}(P-5.78)(PD-365) \quad (3)$$

All dependent variables have a significant effect on the *DS*, accounting for a percentage of the variance in the same order of magnitude (Table 4). The *DS* increases with *P*, up to 560 W L^{-1}, then it decreases with the increase of *P* (Eq. (3)). As *P* increases, US generates more cavitation bubbles, which increases *V* (Schieppati et al., 2024). It suggests that above a certain pressure threshold, cavitation promotes radicals' formation, thus glycosidic bonds and/or esters cleavage, decreasing the *DS* (Liu et al., 2022; Stefanovic et al., 2013).

For esters produced with US and for which the *DS* was determined by gravimetric analysis, the regression (Fig. 12) resulted in the following equation:

$$DS = 0.437 - 0.108{\cdot}\frac{T-60}{20} + 0.249{\cdot}\left(\frac{T-60}{20}\right)^{2} -0.179{\cdot}(P-5.93)^{2} + 1.86{\cdot}10^{-2}{\cdot}\left(\frac{T-60}{20}\right) (P-5.93) + 5.02{\cdot}10^{-3}{\cdot}(P-5.93)(PD-192) \quad (4)$$

The effect of US on the *DS* is similar to that of the previous DoE. All dependent variables have a significant effect on the *DS*, accounting for a percentage of the variance in the same order of magnitude (Table 5). The *DS* increases with *P*, up to 5.93 W, then decreases with the increase of *P* (Eq. (4)). However, the *DS* values are substantially higher when determined by the gravimetric analysis than by ^{1}H NMR HRMAS analysis (Table 1). This discrepancy can be attributed to an underestimation of *DS* by ^{1}H NMR, as the quantification heavily depends on the surface being analyzed and the dissolution extent of the sample. During sample preparation, incomplete dissolution suggests that primarily the surface's groups were quantified (Crépy et al., 2009; Niu et al., 2019). The limitation of solubility as the *DS* increases is attributed to partial cross-linking of sugar rings depolymerized, as evidenced by the formation of a

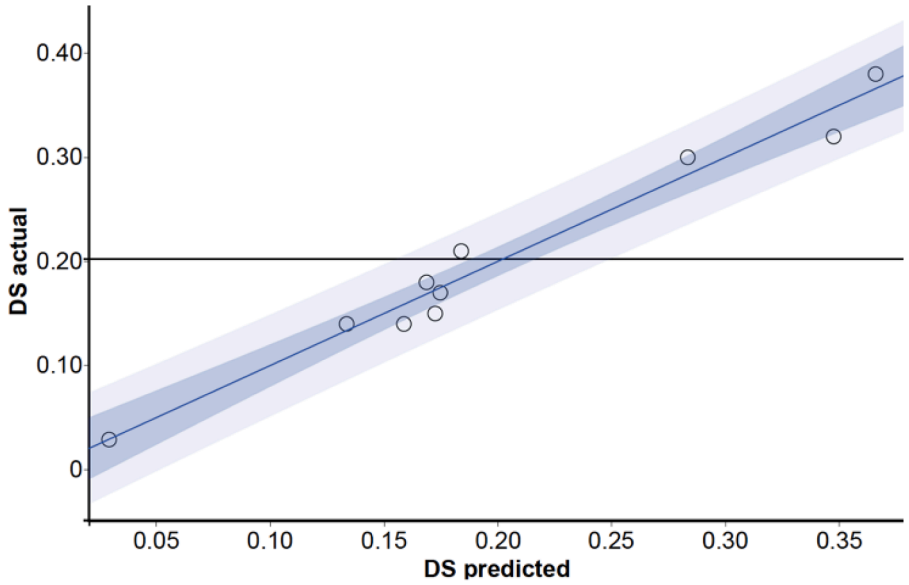

Fig. 11. Actual vs. predicted DS (○) determined by ^{1}H NMR analysis for esters produced with US. Prediction interval.

Table 4
Predictor screening analysis of *DS* determined by ^{1}H NMR analysis for esters produced with US.

Predictor	Portion*
Temperature	63.4 %
PD	23.7 %
P	12.9 %

* Portion of the variance from the prediction.

gel during precipitation (Liu et al., 2022; Stefanovic et al., 2013).

Hou et al. (2023) increased US intensity from 0 to 300 W m^{-2} resulting in a 281 % raise in the *DS* from 0.38 to 1.42. However, MCC had to be regenerated because its crystalline structure and intra and intermolecular hydrogen bonds reduced reactivity. Pretreatment liberated hydroxyl groups, but cellulose fibers still aggregated. Acoustic cavitation broke aggregates, with higher US intensity enhancing the effect.

Lease et al. (2021) esterified cellulose with oleic acid under ball milling for 4 h and 24 h, decreasing the *DS*, from 0.030 to 0.001. The drop in *DS* arises from simultaneous competing reaction, that are esterification and ester hydrolysis by water produced during esterification (Freire et al. (2006)). The hypothesis that the *DS* decreases due to hydrolysis of esters formed is less conceivable in our case, as it is usually promoted in basic medium (Ahmed et al., 2017). In this study, it is assumed that above a certain pressure threshold, cavitation promotes

Table 5
Predictor screening analysis of *DS* determined by gravimetric analysis for esters produced with US.

Predictor	Portion*
Temperature	82.8 %
PD	10.0 %
P	7.20 %

* Portion of the variance from the prediction.

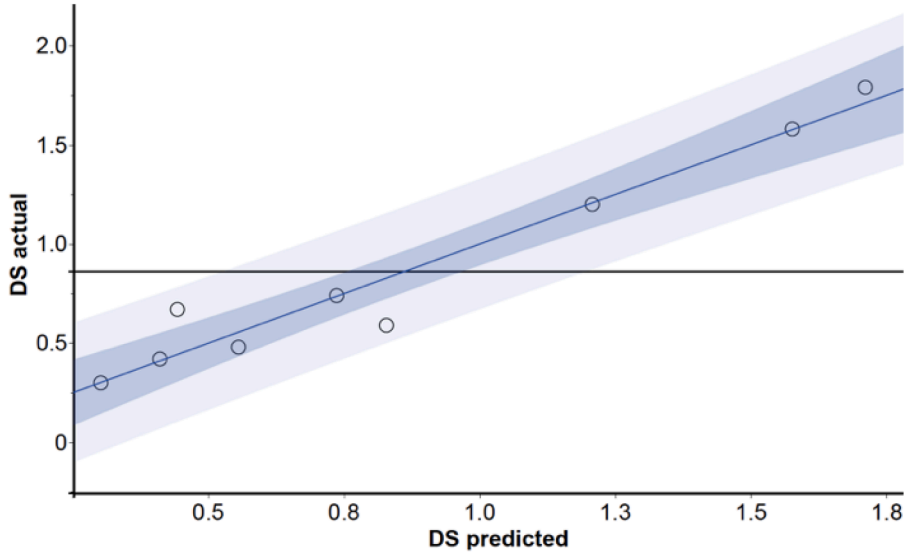

Fig. 12. Actual vs. predicted DS (○) determined by gravimetric analysis for esters produced with US. – Regression, ■ 95 % CI of prediction, RMSE = 0.200, R^2 = 0.947, p-value < 0.0001, – Mean of response (0.863), ■ Prediction interval.

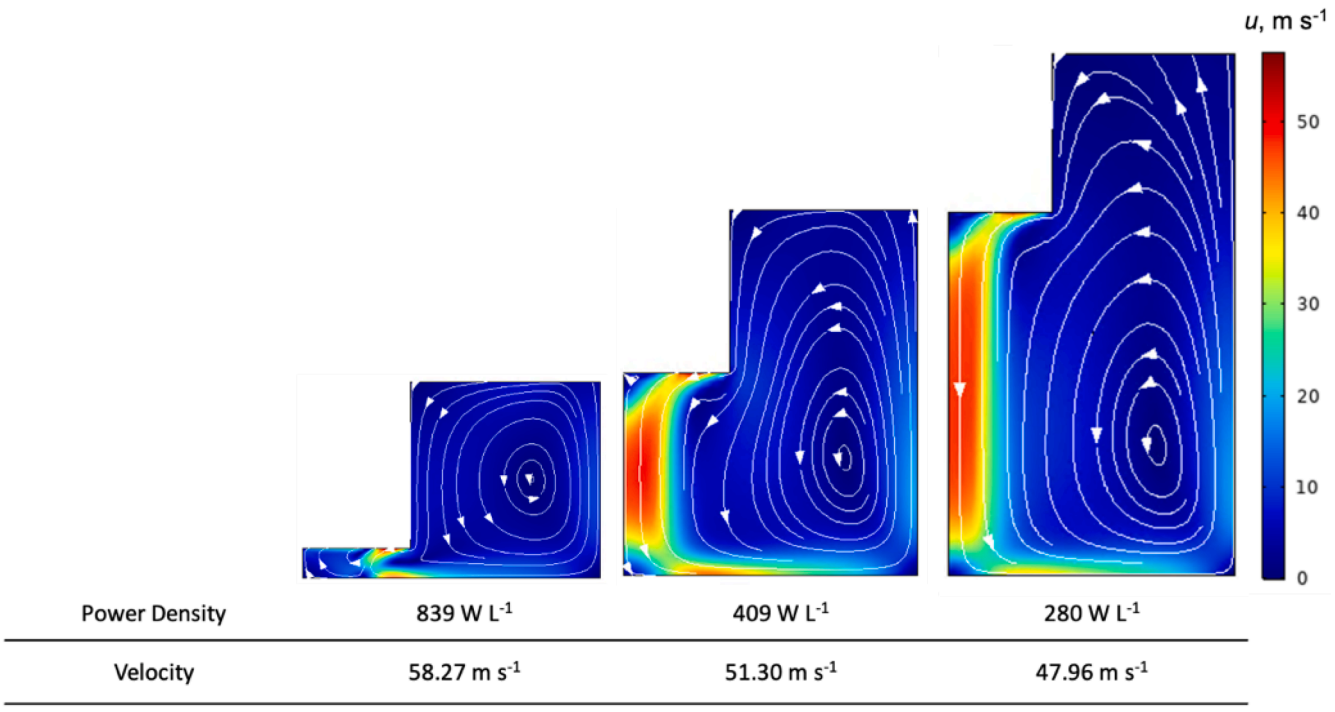

Fig. 13. u of cellulose esters' reaction at 25 g L^{-1} at 9.01 W. u decreases with the increase of reaction's volume.

radicals' formation, thus glycosidic bonds and/or esters cleavage, decreasing the *DS* (Liu et al., 2022; Stefanovic et al., 2013).

4.4. Effect of ultrasound power and power density

Equations (3) and (4), predicting the *DS* from ^{1}H NMR and gravimetric analysis, follow the same trend, indicating a correlation between *P* and *PD*. *DS* determined by ^{1}H NMR analysis increases with *PD* up to 4.80 W and *P* up to 560 W L^{-1}, then it decreases (Eq. (3)). Whereas *DS* determined by gravimetric analysis increases with *P* up to 5.93 W, then it decreases, too (Eq. (4)).

The decrease in *DS* suggests the hydrolysis (de-esterification) and reformation of hydroxyl groups of cellulose. In our process, above 5.93 W, which correspond to 4.47 W cm^{-2}, the locally high temperature and pressure generated by US promote the cleavage of glucose rings and its conversion into pyrazines (Zhang et al., 2022).

Cavitation bubbles grow under positive pressure, collapse and release energy under negative pressure. Simulations determined that at 25 g L^{-1} of cellulose and 20 °C, p_{min} decreases with the increase of *P* (for instance by 43 % from 4.39 W to 9.01 W at 32.2 mL) and rises as *v* decreases (e.g. by 99 % from 32.2 mL to 10.7 mL at 9.01 W). A statistical analysis revealed that p_{min} decreases with the increase of *PD* below 19.4 mL and increases above the threshold:

$$p_{min} = 1.59{\cdot}10^{5} - 8.89{\cdot}10^{3}{\cdot}v + 94.9{\cdot}PD - 3.32{\cdot}10^{3}{\cdot}(P-6.70)(v-21.5) + 46.5{\cdot}(v-21.5)(PD-382) \quad (5)$$

p_{max} is located directly under the tip of the US probe and increases as *P* increases. p_{max} increases as *PD* increases, up to 7.84 W and then decreases (Eq.(6)). The reaction volume does not have a significant effect on p_{max} with only 4 % of the variance. As *P* increases, the energy transferred to the fluid increases, as does the amplitude of the sound waves, then the acoustic pressure.

$$p_{max} = 1.84{\cdot}10^{5} + 2.78{\cdot}10^{4}{\cdot}P + 13.1{\cdot}PD - 208{\cdot}(P-6.70)(v-21.5) - 12.2{\cdot}(P-6.70)(PD-382) \quad (6)$$

Cavitation bubbles accumulate at the vicinity of the probe emitting surface, which attenuates the propagation of sound waves. When the attenuation due to cavitation bubbles is included into the model, this reduces the volume of cavitation zones by 86 % to 99 %. *V* increases as *P* increases up to a reaction volume of 21.5 mL, and then decreases. Instead, *V* decreases as the *PD* increases up to a reaction volume of 16.6 mL, and then increases. The increase of input US power generates more and larger cavitation bubbles, which collapse more frequently and intensely, which increases *V*. On the other hand, as the fluid's volume decreases, so does the fluid's height between the tip of the probe and the bottom wall (keeping the immersion depth constant). The fluid's height is three times less than the wavelength; thus, bubbles have less time to collapse, which reduces cavitation zones volume (Rashwan et al., 2020). Sivakumar and Pandit (2001) observed the same trend, with the increase of cavitation activity up to a maximum, followed by a decrease because of the lower fluid's volume, hence fluid's height. Above 16.6 mL, the increase in *V* is dependent on the increase of *PD*, whereas below 16.6 mL, the decrease in *V* is dependent on the decrease of fluid's volume.

u increases with *PD* (20 % increase from 136 W L^{-1} to 280 W L^{-1} at 32.2 mL), and with the decrease of *v* (22 % drop from 32.2 mL to 10.5 mL at 9.01 W) (Fig. 13). The increase of input US power increases the acoustic pressure amplitude, which in turn increases the volumetric force (Eq.(11) in section S4), resulting in higher *u*. The interaction of acoustic waves with the acoustic streaming also increases *u*. *u* increases with the decrease of *v* (which decreases the fluid's height). Xu et al. (2013) and Laajimi et al. (2022) observed a different effect, with the maximum acoustic streaming velocity increasing with the fluid's height, reaching a peak, and decreasing. They attributed the decrease of velocity to the attenuation due to the liquid height (Xu et al., 2013).

The simulation with the lowest *V* and *u* corresponds to the experimental parameters that produced the highest *DS* values. In contrast, the simulation resulting in the second highest *u* produced the lowest *DS*. The lowest *DS* obtained is in 10.5 mL of reaction mixture. As the probe is located near the bottom of the vessel, the bottom wall reflects the US waves, possibly resulting in a lower mixing efficiency than in 32.2 mL (although simulations gave a higher *u*) (Laajimi et al. (2022)). The cavitation intensity (number and size of bubbles) increases with the *PD*

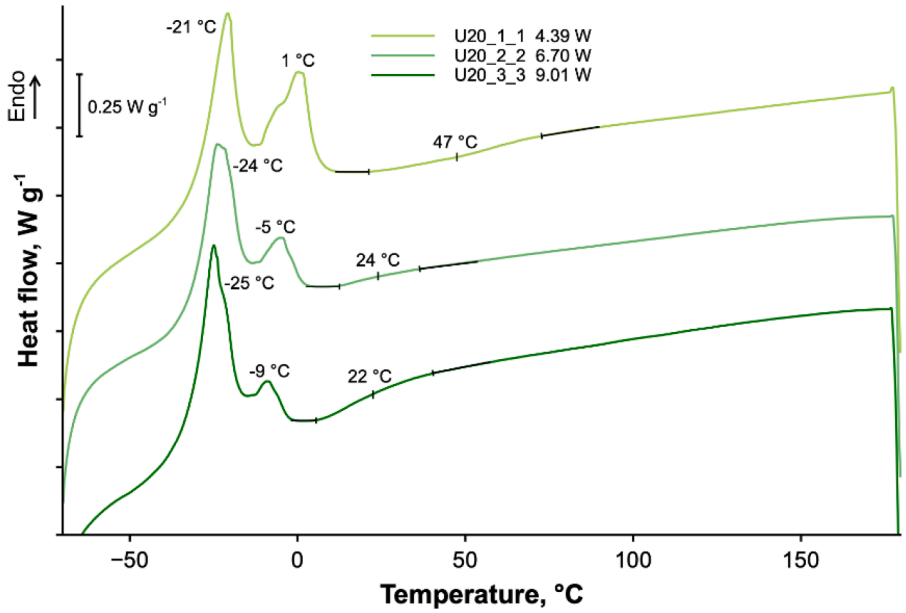

Fig. 14. DSC curves of cellulose esters produced at 20 °C at various US powers.

but becomes too high above 255 W L^{-1}: at the tip of the probe, the bubbles collapse generate less radicals (Fattahi et al., 2022). It is also hypothesized that excessive high velocities generate bubbles in the reactor that form between the reagent molecules, preventing their contact and hindering the reaction.

At a reaction temperature of 20 °C and in a volume of 32.2 mL, two endothermic peaks between −25 °C to −21 °C and between −9 °C to 1 °C are present, followed by a subtle change in T_g (Fig. 14). The first endothermic peak is attributed to the melting of crystals formed by alkyl side chains of FFA. The first peak T_m decreases by 4 °C with the US power. The second endothermic peak is ascribed to the melting of a highly viscous liquid crystalline phase formed during the cooling (Yamagishi et al., 1991). The area of this second melting peak decreases by 77 % with the increase of US power and decrease of *DS*, suggesting a decrease in the amount and/or size of liquid crystals. The two endothermic peaks suggest a polymorphic behaviour with various crystals sizes and arrangements. The T_g increases from 22 °C to 47 °C as the US power decreases from 9.01 W to 4.39 W and as the *DS* increases from 1.20 to 1.79 (Fig. 14). It is attributed to the increase of steric hindrance. However, there is no clear evidence of the trend of T_g with the *DS* (Hou et al., 2023). Thus, the conclusion is that the *PD* does not have a clear effect on the T_g and fusion peak (Figure S6).

5. Conclusion

This work aimed at producing cellulose esters using long chain fatty acids as a green esterification agent and ultrasound (US) as an alternative energy vector to decrease the reaction's energy requirements. Prior to US-assisted esterification, oleic acid and stearic acid were used to esterify two sources of cellulose in silent conditions, at various temperatures. Among conventional esterification samples, the reaction at 80 °C for 24 h resulted in the highest *DS* of 1.44. Among US-assisted esterification samples, the reaction at 20 °C and 136 W L^{-1} for 30 min resulted in the highest *DS* of 0.38 (1.79 determined by gravimetric analysis). The conventionally esterified sample required 93 W g^{-1} of cellulose whereas the US-esterified sample required 18 W g^{-1} of cellulose to achieve the same *DS*. The sample prepared with US displayed a thermoplastic behavior, as confirmed by DSC, with a T_g at 47 °C.

The cavitation activity was characterized with COMSOL Multiphysics 6.1 in cellulose esters solution in a horn-type cylindrical ultrasonic reactor. A temperature of 20 °C, a cellulose concentration of 25 g L^{-1}, an US power of 4.39 W in 32.2 mL were the conditions resulting in the highest *DS* in US-assisted esterification. However, the simulation with these parameters resulted in the smallest active cavitation volume (*V*) and the lowest acoustic streaming velocity (*u*): $9.60 \cdot 10^{-8}$ m^3 and 40.06 m s^{-1}. This shows the critical role of localized cavitation and nonlinear phenomena in driving esterification, underscoring the importance of refining multiphysics models for US-assisted reactions. Overall, these findings provide a clear proof that US significantly reduces energy input, enables room temperature processing and produces functional thermoplastic cellulose esters. This work paves the way for new process development, integrating ionic liquids as solvent and catalyst systems, and kinetic modeling of ester formation. The demonstrated energy efficiency and material performance support US as an intensification strategy for cellulose functionalization, directly addressing sustainability.

CRediT authorship contribution statement

Pierre Dal: Writing – original draft, Software, Methodology, Investigation, Formal analysis, Data curation, Conceptualization. **Annelise Jean-Fulcrand:** Writing – review & editing. **Jean-Marc Lévêque:** Writing – review & editing. **Jean-Marie Raquez:** Writing – review & editing, Supervision. **Daria C. Boffito:** Writing – review & editing, Validation, Supervision, Resources, Funding acquisition, Conceptualization.

Declaration of competing interest

The authors declare that they have no known competing financial interests or personal relationships that could have appeared to influence the work reported in this paper.

Acknowledgements

The authors are thankful to Cédric Malveau for providing assistance during the nuclear magnetic resonance experiments. The authors are thankful to Jean Provost and his group for the material for speed of sound measurements. Pierre Dal is thankful to Institut de l'Energie Trottier, and MITACS, for awarding him graduate scholarships to support his studies. The authors are thankful to Dalma Schieppati for advices about designs of experiment and simulations. This work was

undertaken, in part, thanks to the support of the NSERC - Natural Sciences and Engineering Research Council and of the Canada Research Chairs.

Supplementary materials

Supplementary material associated with this article can be found, in the online version, at doi:10.1016/j.clce.2025.100209.

Data availability

Data will be made available on request.

References

Abdul Hadi, N., Wiege, B., Stabenau, S., Marefati, A., Rayner, M., 2020. Comparison of three methods to determine the degree of substitution of quinoa and rice starch acetates, propionates, and butyrates: direct stoichiometry, FTIR, and 1H-NMR. Foods. 9, 83. https://doi.org/10.3390/foods9010083.

Ahmed, F., Ayoub Arbab, A., Jatoi, A.W., Khatri, M., Memon, N., Khatri, Z., Kim, I.S., 2017. Ultrasonic-assisted deacetylation of cellulose acetate nanofibers: a rapid method to produce cellulose nanofibers. Ultrason. Sonochem. 36, 319–325. https://doi.org/10.1016/j.ultsonch.2016.12.013.

Almasi, H., Ghanbarzadeh, B., Dehghannia, J., Pirsa, S., Zandi, M., 2015. Heterogeneous modification of softwoods cellulose nanofibers with oleic acid: effect of reaction time and oleic acid concentration. Fibers Polym. 16, 1715–1722. https://doi.org/10.1007/s12221-015-4294-1.

Barthel, S., Heinze, T., 2006. Acylation and carbanilation of cellulose in ionic liquids. Green. Chem. 8, 301–306. https://doi.org/10.1039/B513157J.

Bhaumik, P., Dhepe, P.L., 2015. Conversion of biomass into sugars. Biomass Sugars for Non-Fuel Applications. The Royal Society of Chemistry, pp. 1–53. https://doi.org/10.1039/9781782622079-00001.

Bochek, A.M., 2003. Effect of hydrogen bonding on cellulose solubility in aqueous and nonaqueous solvents. Russ. J. Appl. Chem. 76, 1711–1719. https://doi.org/10.1023/B:RJAC.0000018669.88546.56.

Boffito, D.C., Galli, F., Pirola, C., Bianchi, C.L., Patience, G.S., 2014. Ultrasonic free fatty acids esterification in tobacco and canola oil. Ultrason. Sonochem. 21, 1969–1975. https://doi.org/10.1016/j.ultsonch.2014.01.026.

Commander, K.W., Prosperetti, A., 1989. Linear pressure waves in bubbly liquids: comparison between theory and experiments. J. Acoust. Soc. Am. 85, 732–746. https://doi.org/10.1121/1.397599.

Costa, C., Silva, C., Marques, E.F., Azoia, N.G., 2023. Long-chain cellulose esters from recycling textile waste as highly effective superhydrophobic additive: synthesis and evaluation. Cellulose 30, 2913–2928. https://doi.org/10.1007/s10570-023-05065-3.

Crépy, L., Chaveriat, L., Banoub, J., Martin, P., Joly, N., 2009. Synthesis of cellulose fatty esters as plastics—Influence of the degree of substitution and the fatty chain length on mechanical properties. ChemSusChem. 2, 165–170. https://doi.org/10.1002/cssc.200800171.

Daulay, I.R.S., Ariyanta, H.A., Karimah, A., Fitria, Santoso, E.B., Cahyana, A.H., Bukhari, M.N.S.S., Bakshi, M.I., Dungani, R., Hanifa, T.Z., Karliati, T., Farobie, O., Iswanto, A.H., Fatriasari, W., 2024. Preparation of superhydrophobic biomedical pulp from rice straw coated with a stearic acid-cellulose composite. Bioresour. Technol. Rep. 25, 101781. https://doi.org/10.1016/j.biteb.2024.101781.

Duchatel-Crépy, L., Joly, N., Martin, P., Marin, A., Tahon, J.-F., Lefebvre, J.-M., Gaucher, V., 2020. Substitution degree and fatty chain length influence on structure and properties of fatty acid cellulose esters. Carbohydr. Polym. 234, 115912. https://doi.org/10.1016/j.carbpol.2020.115912.

Edgar, K.J., Buchanan, C.M., Debenham, J.S., Rundquist, P.A., Seiler, B.D., Shelton, M.C., Tindall, D., 2001. Advances in cellulose ester performance and application. Prog. Polym. Sci. 26, 1605–1688. https://doi.org/10.1016/S0079-6700(01)00027-2.

Fattahi, K., Robert, E., Boffito, D.C., 2022. Numerical and experimental investigation of the cavitation field in horn-type sonochemical reactors. Chem. Eng. Process. - Process Intensif. 182, 109186. https://doi.org/10.1016/j.cep.2022.109186.

Fernandez Rivas, D., Boffito, D.C., Faria-Albanese, J., Glassey, J., Afraz, N., Akse, H., Boodhoo, Kamelia.V.K., Bos, R., Cantin, J., (Emily) Chiang, Y.W., Commenge, J.-M., Dubois, J.-L., Galli, F., de Mussy, J.P.G., Harmsen, J., Kalra, S., Keil, F.J., Morales-Menendez, R., Navarro-Brull, F.J., Noël, T., Ogden, K., Patience, G.S., Reay, D., Santos, R.M., Smith-Schoettker, A., Stankiewicz, A.I., van den Berg, H., van Gerven, T., van Gestel, J., van der Stelt, M., van de Ven, M., Weber, R.S., 2020. Process intensification education contributes to sustainable development goals. Part 1. Educ. Chem. Eng. 32, 1–14. https://doi.org/10.1016/j.ece.2020.04.003.

Ferro, M., Castiglione, F., Panzeri, W., Dispenza, R., Santini, L., Karlsson, H.J., de Wit, P. P., Mele, A., 2017. Non-destructive and direct determination of the degree of substitution of carboxymethyl cellulose by HR-MAS 13C NMR spectroscopy. Carbohydr. Polym. 169, 16–22. https://doi.org/10.1016/j.carbpol.2017.03.097.

Freire, C.S.R., Silvestre, A.J.D., Neto, C.P., Belgacem, M.N., Gandini, A., 2006. Controlled heterogeneous modification of cellulose fibers with fatty acids: effect of reaction conditions on the extent of esterification and fiber properties. J. Appl. Polym. Sci. 100, 1093–1102. https://doi.org/10.1002/app.23454.

García-Zapateiro, L.A., Franco, J.M., Valencia, C., Delgado, M.A., Gallegos, C., 2013. Viscous, thermal and tribological characterization of oleic and ricinoleic acids-derived estolides and their blends with vegetable oils. J. Ind. Eng. Chem. 19, 1289–1298. https://doi.org/10.1016/j.jiec.2012.12.030.

Goris, Q., Bampouli, A., Noorul Hussain, M., Louisnard, O., Stefanidis, G.D., Van Gerven, T., 2025. A new strategy for modelling sonochemical reactors: coupling of the non-linear Louisnard model with mass and heat transport equations with applications to cavitating viscous fluids. Ultrason. Sonochem. 112, 107114. https://doi.org/10.1016/j.ultsonch.2024.107114.

Grönroos, A., Pirkonen, P., Ruppert, O., 2004. Ultrasonic depolymerization of aqueous carboxymethylcellulose. Ultrason. Sonochem. 11, 9–12. https://doi.org/10.1016/S1350-4177(03)00129-9.

Habibi, Y., 2014. Key advances in the chemical modification of nanocelluloses. Chem. Soc. Rev. 43, 1519–1542. https://doi.org/10.1039/C3CS60204D.

Haouache, S., Karam, A., Chave, T., Clarhaut, J., Amaniampong, P.N., Garcia Fernandez, J.M., De Oliveira Vigier, K., Capron, I., Jérôme, F., 2020. Selective radical depolymerization of cellulose to glucose induced by high frequency ultrasound. Chem. Sci. 11, 2664–2669. https://doi.org/10.1039/D0SC00020E.

Heinze, T., 2015. Cellulose: structure and properties. Cellulose Chemistry and Properties: Fibers, Nanocelluloses and Advanced Materials. Springer, Cham, pp. 1–52. https://doi.org/10.1007/12_2015_319.

Heinze, T., El Seoud, O., Koschella, A., 2018. Cellulose Derivatives: Synthesis, Structure, and Properties. Springer.

Heinze, T., Liebert, T., Koschella, A., 2006. Esterification of Polysaccharides. Springer-Verlag, Berlin/Heidelberg. https://doi.org/10.1007/3-540-32112-8.

Hou, D.-F., Li, M.-L., Yan, C., Zhou, L., Liu, Z.-Y., Yang, W., Yang, M.-B., 2021. Mechanochemical preparation of thermoplastic cellulose oleate by ball milling. Green Chem. 23, 2069–2078. https://doi.org/10.1039/D0GC03853A.

Hou, D.-F., Yuan, P.-P., Feng, Z.-W., An, M., Li, P.-Y., Liu, C., Yang, M.-B., 2023. Sustainable conversion regenerated cellulose into cellulose oleate by sonochemistry. Front. Chem. Sci. Eng. 17, 1096–1108. https://doi.org/10.1007/s11705-023-2317-9.

Huang, L., Wu, Q., Wang, Q., Wolcott, M., 2019. One-step activation and surface fatty acylation of cellulose fibers in a solvent-free condition. ACS. Sustain. Chem. Eng. 7, 15920–15927. https://doi.org/10.1021/acssuschemeng.9b01974.

Jandura, P., Kokta, B.V., Riedl, B., 2000a. Fibrous long-chain organic acid cellulose esters and their characterization by diffuse reflectance FTIR spectroscopy, solid-state CP/MAS13C-NMR, and X-ray diffraction. J. Appl. Polym. Sci. 78, 1354–1365. https://doi.org/10.1002/1097-4628(20001114)78:7<1354::AID-APP60>3.0.CO;2-V.

Jandura, P., Riedl, B., Kokta, B.V., 2000b. Thermal degradation behavior of cellulose fibers partially esterified with some long chain organic acids. Polym. Degrad. Stab. 70, 387–394. https://doi.org/10.1016/S0141-3910(00)00132-4.

Jebrane, M., Terziev, N., Heinmaa, I., 2017. Biobased and sustainable alternative route to long-chain cellulose esters. Biomacromolecules. 18, 498–504. https://doi.org/10.1021/acs.biomac.6b01584.

Joyce Tiong, T., Chu, J.K., Tan, K.W., 2025. Advancements in acoustic cavitation modelling: progress, challenges, and future directions in sonochemical reactor design. Ultrason. Sonochem. 112, 107163. https://doi.org/10.1016/j.ultsonch.2024.107163.

Kulomaa, T., Matikainen, J., Karhunen, P., Heikkilä, M., Fiskari, J., Kilpeläinen, I., 2015. Cellulose fatty acid esters as sustainable film materials – effect of side chain structure on barrier and mechanical properties. RSC. Adv. 5, 80702–80708. https://doi.org/10.1039/C5RA12671A.

Laajimi, H., Fattahi, K., Boffito, D.C., 2022. Numerical investigation of the ultrasound-assisted biodiesel transesterification with a polyalcohol. Chem. Eng. Process. - Process Intensif. 181, 109139. https://doi.org/10.1016/j.cep.2022.109139.

Lan, W., Liu, C.-F., Yue, F.-X., Sun, R.-C., Kennedy, J.F., 2011. Ultrasound-assisted dissolution of cellulose in ionic liquid. Carbohydr. Polym. 86, 672–677. https://doi.org/10.1016/j.carbpol.2011.05.013.

Lease, J., Kawano, T., Andou, Y., 2021. Esterification of cellulose with long fatty acid chain through mechanochemical method. Polym. (Basel) 13, 4397. https://doi.org/10.3390/polym13244397.

Li, A., Zhong, R., Li, X., Zhang, J., 2020. Enhancement of sonochemical efficiency using combination of ultrasound with ultraviolet irradiation and water flow in a horn-type reactor. Chem. Eng. Process. - Process Intensif. 150, 107884. https://doi.org/10.1016/j.cep.2020.107884.

Liang, P., Chen, C., Zhao, S., Ge, F., Liu, D., Liu, B., Fan, Q., Han, B., Xiong, X., 2013. Application of fourier transform infrared spectroscopy for the oxidation and peroxide value evaluation in Virgin walnut oil. J. Spectrosc. 2013, 1–5. https://doi.org/10.1155/2013/138728.

Lindman, B., Karlström, G., Stigsson, L., 2010. On the mechanism of dissolution of cellulose. J. Mol. Liq. 156, 76–81. https://doi.org/10.1016/j.molliq.2010.04.016.

Liu, C.F., Sun, R.C., Qin, M.H., Zhang, A.P., Ren, J.L., Ye, J., Luo, W., Cao, Z.N., 2008. Succinoylation of sugarcane bagasse under ultrasound irradiation. Bioresour. Technol. 99, 1465–1473. https://doi.org/10.1016/j.biortech.2007.01.062.

Liu, Y., Li, S., Wang, Z., Wang, L., 2022. Ultrasound in cellulose-based hydrogel for biomedical use: from extraction to preparation. Colloids. Surf. B Biointerfaces. 212, 112368. https://doi.org/10.1016/j.colsurfb.2022.112368.

Ma, S., Xue, X., Yu, S., Wang, Z., 2012. High-intensity ultrasound irradiated modification of sugarcane bagasse cellulose in an ionic liquid. Ind. Crops. Prod. 35, 135–139. https://doi.org/10.1016/j.indcrop.2011.06.023.

Ma, S., Yu, S., Wang, Z., Zheng, X., 2013. Ultrasound-assisted modification of beet pulp cellulose with phthalic anhydride in ionic liquid. Cellul. Chem. Technol. 47, 527–533.

Meroni, D., Djellabi, R., Ashokkumar, M., Bianchi, C.L., Boffito, D.C., 2022. Sonoprocessing: from concepts to large-scale reactors. Chem. Rev. 122, 3219–3258. https://doi.org/10.1021/acs.chemrev.1c00438.

Mikkola, J.-P., Kirilin, A., Tuuf, J.-C., Pranovich, A., Holmbom, B., Kustov, L.M., Murzin, D.Yu., Salmi, T., 2007. Ultrasound enhancement of cellulose processing in ionic liquids: from dissolution towards functionalization. Green Chem. 9, 1229. https://doi.org/10.1039/b708533h.

Mikkola, J.-P., Toukoniitty, B., Toukoniitty, E., Aumo, J., Salmi, T., 2004. Utilisation of on-line acoustic irradiation as a means to counter-effect catalyst deactivation in heterogeneous catalysis. Ultrason. Sonochem. 11, 233–239. https://doi.org/10.1016/j.ultsonch.2004.01.020.

Morselli Ribeiro, M.D.M., Barrera Arellano, D., Ferreira Grosso, C.R., 2012. The effect of adding oleic acid in the production of stearic acid lipid microparticles with a hydrophilic core by a spray-cooling process. Food Res. Int. 47, 38–44. https://doi.org/10.1016/j.foodres.2012.01.007.

Niu, X., Liu, Y., King, A.W.T., Hietala, S., Pan, H., Rojas, O.J., 2019. Plasticized cellulosic films by partial esterification and welding in low-concentration ionic liquid electrolyte. Biomacromolecules. 20, 2105–2114. https://doi.org/10.1021/acs.biomac.9b00325.

Olympus, n.d. Vitesse de propagation des ondes ultrasonores dans les matériaux [WWW Document]. https://www.olympus-ims.com/fr/ndt-tutorials/thickness-gauge/appendices-velocities/.

Rashwan, S.S., Dincer, I., Mohany, A., 2020. Investigation of acoustic and geometric effects on the sonoreactor performance. Ultrason. Sonochem. 68, 105174. https://doi.org/10.1016/j.ultsonch.2020.105174.

Rustan, A.C., Drevon, C.A., 2005. Fatty acids: structures and properties. Encyclopedia of Life Sciences. Wiley. https://doi.org/10.1038/npg.els.0003894.

Schieppati, D., Mohan, M., Blais, B., Fattahi, K., Patience, G.S., Simmons, B.A., Singh, S., Boffito, D.C., 2024. Characterization of the acoustic cavitation in ionic liquids in a horn-type ultrasound reactor. Ultrason. Sonochem. 102, 106721. https://doi.org/10.1016/j.ultsonch.2023.106721.

Sealey, J.E., Samaranayake, G., Todd, J.G., Glasser, W.G., 1996. Novel cellulose derivatives. IV. Preparation and thermal analysis of waxy esters of cellulose. J. Polym. Sci. B Polym. Phys. 34, 1613–1620. https://doi.org/10.1002/(SICI)1099-0488(19960715)34:9<1613::AID-POLB10>3.0.CO;2-A.

Sejati, P.S., Obounou Akong, F., Fradet, F., Gérardin, P., 2024a. Understanding the thermoplasticization mechanism of wood via esterification with fatty acids: a comparative study of the reactivity of cellulose, hemicelluloses and lignin. Carbohydr. Polym. 324, 121542. https://doi.org/10.1016/j.carbpol.2023.121542.

Sejati, P.S., Obounou Akong, F., Torloting, C., Fradet, F., Gérardin, P., 2023. Thermoplastic translucent film from wood and fatty acids by solvent free esterification: influence of fatty acid chain length. Eur. Polym. J. 196, 112276. https://doi.org/10.1016/j.eurpolymj.2023.112276.

Sejati, P.S., Roche, L., Afrim, J., Mariani, V., Akong, F.O., Fradet, F., Gérardin, P., 2024b. Thermoplastic film from natural fibers and fatty acids by a single esterification reaction. Cellulose 31, 4263–4276. https://doi.org/10.1007/s10570-024-05865-1.

Sivakumar, M., Pandit, A.B., 2001. Ultrasound enhanced degradation of rhodamine B: optimization with power density. Ultrason. Sonochem. 8, 233–240. https://doi.org/10.1016/S1350-4177(01)00082-7.

Stefanovic, B., Rosenau, T., Potthast, A., 2013. Effect of sonochemical treatments on the integrity and oxidation state of cellulose. Carbohydr. Polym. 92, 921–927. https://doi.org/10.1016/j.carbpol.2012.09.039.

Suslick, K.S., 1990. Sonochemistry. Sci. (1979) 247, 1439–1445. https://doi.org/10.1126/science.247.4949.1439.

Tanaka, S., Iwata, T., Iji, M., 2017. Long/short chain mixed cellulose esters: effects of Long acyl chain structures on mechanical and thermal properties. ACS. Sustain. Chem. Eng. 5, 1485–1493. https://doi.org/10.1021/acssuschemeng.6b02066.

Tang, L., Huang, B., Lu, Q., Wang, S., Ou, W., Lin, W., Chen, X., 2013. Ultrasonication-assisted manufacture of cellulose nanocrystals esterified with acetic acid. Bioresour. Technol. 127, 100–105. https://doi.org/10.1016/j.biortech.2012.09.133.

Tarasova, E., Krasnou, I., Enkhsaikhan, G., Abousharabia, I., Nunes, C.C.Z., Karthegesu, D., Savale, N., Kontturi, E., Krumme, A., 2024. Reactive extrusion of cellulose esters in ionic liquid: exploring properties and performance across different cellulose types and degrees of polymerization. Cellulose. https://doi.org/10.1007/s10570-024-06203-1.

Uschanov, P., Johansson, L.-S., Maunu, S.L., Laine, J., 2011. Heterogeneous modification of various celluloses with fatty acids. Cellulose 18, 393–404. https://doi.org/10.1007/s10570-010-9478-7.

Vaca-Garcia, C., Borredon, M.E., 1999. Solvent-free fatty acylation of cellulose and lignocellulosic wastes. Part 2: reactions with fatty acids1The first paper of this series is: thiebaud, S., Borredon, M.E., 1995. Solvent-free wood esterification with fatty acid chlorides. Bioresour. Technol 52, 169–173. https://doi.org/10.1016/S0960-8524(99)00034-6, 1. Bioresour Technol 70, 135–142.

Wang, H., Gurau, G., Rogers, R.D., 2012. Ionic liquid processing of cellulose. Chem. Soc. Rev. 41, 1519. https://doi.org/10.1039/c2cs15311d.

Willberg-Keyriläinen, P., Ropponen, J., 2019. Evaluation of esterification routes for long chain cellulose esters. Heliyon. 5. https://doi.org/10.1016/j.heliyon.2019.e02898 e02898.

Willberg-Keyriläinen, P., Talja, R., Asikainen, S., Harlin, A., Ropponen, J., 2016. The effect of cellulose molar mass on the properties of palmitate esters. Carbohydr. Polym. 151, 988–995. https://doi.org/10.1016/j.carbpol.2016.06.048.

Xu, Z., Yasuda, K., Koda, S., 2013. Numerical simulation of liquid velocity distribution in a sonochemical reactor. Ultrason. Sonochem. 20, 452–459. https://doi.org/10.1016/j.ultsonch.2012.04.011.

Yamagishi, T., Fukuda, T., Miyamoto, T., Takashina, Y., Yakoh, Y., Watanabe, J., 1991. Thermotropic cellulose derivatives with flexible substituents IV. Columnar liquid crystals from ester-type derivatives of cellulose. Liq. Cryst. 10, 467–473. https://doi.org/10.1080/02678299108036436.

Zhang, Jinming, Chen, W., Feng, Y., Wu, J., Yu, J., He, J., Zhang, Jun, 2015. Homogeneous esterification of cellulose in room temperature ionic liquids. Polym. Int. 64, 963–970. https://doi.org/10.1002/pi.4883.

Zhang, R., Zhang, Y., Sun, Y., Yu, H., Yang, F., Guo, Y., Xie, Y., Yao, W., 2022. High-intensity ultrasound promoted the aldol-type condensation as an alternative mean of synthesizing pyrazines in a Maillard reaction model system of D-glucose-13C6 and L-glycine. Ultrason. Sonochem. 82, 105913. https://doi.org/10.1016/j.ultsonch.2022.105913.

Zheng, Y., Song, J., Cheng, B., Fang, X., Yuan, Y., 2015. Preparation and flame retardancy of 3-(hydroxyphenylphosphinyl)-propanoic acid esters of cellulose and their fibers. Cellulose 22, 229–244. https://doi.org/10.1007/s10570-014-0486-x.